DYNAMIC STALL SIMULATIONS WITH FINITE-VOLUME BASED LATTICE BOLTZMANN METHOD

Goktan Guzel, Bedri Yagiz, and A. Emre Çetiner
MGEO Division, ASELSAN Inc., Ankara, Turkey

Abstract

In this study, the capability of the Lattice-Boltzmann Method (LBM) is demonstrated simulating one of the most challenging problems in rotor aerodynamics, i.e. dynamic stall. For this purpose, 2-D simulations with an in-house developed finite-volume based LBM flow solver were performed for a NACA 0015 airfoil that is sinusoidally pitching around its quarter-chord. For the current study, three cases for different mean angles of attack but with the same pitching amplitude and the frequency were considered. Each case corresponds to different flow regimes, i.e. attached flow, light stall, and deep stall. Once the converged solutions were obtained, the computed variations of forces and pitching moment were compared with the measured data and satisfactory results were obtained. Also, the same simulations were repeated with a NS equations based flow solver that is available commercially (Fluent Version 14.5) and the comparison between the two methods revealed that both provides almost equivalent results.

1. INTRODUCTION

Since its first introduction by McNamara[1] almost thirty years ago, the LBM has become an alternative to the classical Navier-Stokes (NS) equations based methods and its use and applications in various areas are getting increasing acceptance among the Computational Fluid Dynamics (CFD) community, see for example [2], [3], [4], and [5]. Derived from the Lattice-Gas Automata (LGA) method[6], the LBM basically shares the same idea. In the LGA method, which can be thought as a simple Molecular Dynamics model, the gas is modeled as a cluster of solid spheres moving along a uniform lattice. Each solid sphere has a discrete set of possible velocities and the collision between separate particles is handled by a set of elastic collision rules. Macroscopic quantities, such as particle density and velocity at each lattice node, can be computed using the microscopic quantities, making it possible to study the macroscopic behavior of a fluid flow. Numerically, the LGA method suffers the statistical noise caused by the averaging procedure to obtain the macroscopic properties from the microscopic properties. To remedy the statistical noise that the LGA method suffers, the LBM was developed. The main difference between the two methods is that instead of handling single particles, the LBM handles particle distributions. This removes the need for averaging to obtain the macroscopic properties from the microscopic properties, so the statistical noise is also removed. Even though the idea given above is simple, the method still provides similar solutions as the incompressible NS equations based methods do. Beyond being simple, it has several advantages over its counterpart. For example, the equation solved when utilizing the LBM is a first order ordinary differential equation, which is easier to discretize compared to the second order equations of NS equations based methods. In addition, one does not have to solve computationally expensive Poisson equation, which is required when coupling pressure and velocity solutions when using NS equations based methods. Also, since no pressure-velocity coupling is not needed, the complex staggered-grid systems are not required, too. Furthermore, the convective term included in the equation of the LBM is linear, which is easier to handle numerically considering the non-linear convective term included in the NS equations, so the solution effort is reduced further.

In this study, the capability of the Lattice-Boltzmann Method (LBM) is demonstrated simulating one of the most challenging problems in rotor aerodynamics, i.e. dynamic stall. The challenge is due to the complex nature of the flow that involves unsteadiness, separation, reattachment and turbulence which produce harmful effects such as stall flutter and harsh vibrations on overall aircraft system. Dynamic stall appears on helicopter rotor blades too, when the blades are moving opposite direction of the flight and its occurrence seriously limits the forward speed and the maneuverability of helicopters. It occurs when a pitching airfoil exceeds its static-stall angle. Beyond this angle, a disturbance occurs in the boundary layer and it triggers the reverse flow at the trailing edge of the airfoil while it is spreading towards the leading edge. Many factors such as airfoil shape, pitch rate, frequency, Reynolds number, and Mach number could affect this reversal progress. Subsequently, a very strong vortex begins to evolve close to the leading edge of the airfoil. This newborn vortex then moves downstream which gives

rise to a variation of aerodynamic forces and moments over the airfoil surface. It continues to enlarge downstream and then drag starts to increase, while both lift and pitching moment decreases rapidly. There have been numerous researches about this phenomenon in the literature. McCroskey et al.[7] and Piziali[8] experimentally investigated a pitching airfoil to reveal the flow events. Wang et al.[9] numerically investigated the effects of different frequencies, mean oscillating angles and amplitudes at low Reynolds numbers. Recently, Dumlupinar et al.[10] and Fang et al.[11] simulate dynamic stall at different flow conditions using various numerical methods.

For the aim given above, 2-D simulations with an in-house developed finite-volume based LBM flow solver were performed for a NACA 0015 airfoil that is sinusoidally pitching around its quarter-chord. This is the case that was also investigated experimentally by Piziali[8] and the report of this experiment includes data such as the variations of lift and drag forces and pitching moment with the pitch angle. For the current study, three cases for different mean angles of attack but with the same pitching amplitude and the frequency were considered. Each case corresponds to different flow regimes, i.e. attached flow, light stall, and deep stall. Once the converged solutions were obtained, the computed variations of forces and pitching moment were compared with the measured data and satisfactory results were obtained. Also, the same simulations were repeated with a NS equations based flow solver that is available commercially (Fluent Version 14.5) and the comparison between the two methods revealed that both provides almost equivalent results.

2. NUMERICAL METHOD

2.1. Finite-Volume Based Lattice-Boltzmann Method

The present implementation of the LBM follows a cell-centered finite-volume approach. The derivation of the LBM in finite-volume form starts with the discrete velocity Boltzmann Equation, which is given by;

$$\frac{\partial f_\alpha}{\partial t} + \vec{e}_\alpha \cdot \vec{\nabla} f_\alpha = -\frac{1}{\lambda}(f_\alpha - f_\alpha^{eq}), \tag{1}$$

where α stands for the direction of the discrete velocity, $f = f(\vec{x}, \vec{e}, t)$ is the particle distribution function in which $\vec{x}$ is the position vector, $\vec{e}$ is the particle velocity vector, t is the time, f^{eq} is the equilibrium distribution function (or Maxwell-Boltzmann distribution function), and λ is the relaxation time. Then, Eq. (1) is integrated over quadrilateral control volumes that form a structured grid. Considering the Fig. (1), the integration of the first term on the left hand side of Eq. (1) (the unsteady term) over the control volume [i, j] is given as;

$$\int_{abcd} \left(\frac{\partial f_\alpha}{\partial t}\right) dA \approx \left(\frac{\partial f_\alpha}{\partial t}\right)_{[i,j]} A_{[i,j]}, \tag{2}$$

where $A_{[i,j]}$ is the area of the cell that is indexed as [i, j].

For the integration of the second term on the left hand side of Eq. (1) (the advection term), the divergence theorem is applied;

$$\int_{abcd} (\vec{e}_\alpha \cdot \vec{\nabla} f_\alpha) dA = \oint_{abcd} (\vec{e}_\alpha \cdot \vec{n}) f_\alpha dl, \tag{3}$$

where $\vec{n}$ is the unit normal vectors of the edges that form the cell considered. The right hand side of Eq. (3) can be written for a quadrilateral cell as follows;

$$\begin{aligned}\oint_{abcd} (\vec{e}_\alpha \cdot \vec{n}) f_\alpha dl = &\left(\vec{e}_\alpha \cdot \vec{n}(ab)_{[i,j]}\right) f_\alpha(ab)_{[i,j]} l(ab)_{[i,j]} \\ &+ \left(\vec{e}_\alpha \cdot \vec{n}(bc)_{[i,j]}\right) f_\alpha(bc)_{[i,j]} l(bc)_{[i,j]} \\ &+ \left(\vec{e}_\alpha \cdot \vec{n}(cd)_{[i,j]}\right) f_\alpha(cd)_{[i,j]} l(cd)_{[i,j]} \\ &+ \left(\vec{e}_\alpha \cdot \vec{n}(da)_{[i,j]}\right) f_\alpha(da)_{[i,j]} l(da)_{[i,j]},\end{aligned} \tag{4}$$

where *l* terms are the length of each edge that forms the cell considered. For the evaluation of flux-terms introduced in Eq. (4), an interpolation scheme is needed to compute edge values of the distribution functions. For this purpose, the Monotone Upstream-centered Scheme for Conservation Laws (MUSCL)[12] might be used. For example, depending on the sign of the $(\vec{e}_\alpha \cdot \vec{n}(bc)_{[i,j]})$ term, the distribution function on the *bc* edge is given as;

$$f_\alpha(bc)_{[i,j]} = \begin{cases} f_{\alpha[i,j]} + \frac{1}{4}\left((1+\kappa)\cdot(f_{\alpha[i+1,j]} - f_{\alpha[i,j]})\right) \\ \quad + \frac{1}{4}\left((1-\kappa)\cdot(f_{\alpha[i,j]} - f_{\alpha[i-1,j]})\right), \text{ for } \vec{e}_\alpha \cdot \vec{n}(bc)_{[i,j]} \geq 0 \\ f_{\alpha[i+1,j]} + \frac{1}{4}\left((1+\kappa)\cdot(f_{\alpha[i,j]} - f_{\alpha[i+1,j]})\right) \\ \quad + \frac{1}{4}\left((1-\kappa)\cdot(f_{\alpha[i+1,j]} - f_{\alpha[i+2,j]})\right), \text{ for } \vec{e}_\alpha \cdot \vec{n}(bc)_{[i,j]} < 0, \end{cases} \tag{5}$$

where the term κ determines the spatial accuracy and by setting this term to 1/3, one can obtain second order accuracy.

The term on the right hand side of Eq. (1) (the collision term) can be integrated using;

$$-\frac{1}{\lambda}\int_{abcd} (f_\alpha - f_\alpha^{eq}) dA \approx -\frac{1}{\lambda}(f_\alpha - f_\alpha^{eq})_{[i,j]} A_{[i,j]}. \tag{6}$$

So, the finite-volume formulation of the LBM for a sample cell of $abcd$ as shown in Fig. (1) takes the final form given as;

$$\left(\frac{\partial f_\alpha}{\partial t}\right)_{[i,j]} A_{[i,j]} + F_{\alpha[i,j]} = -\frac{1}{\lambda}(f_\alpha - f_\alpha^{eq})_{[i,j]} A_{[i,j]}, \quad (7)$$

where $F_{\alpha[i,j]}$ stands for the flux terms that is introduced in Eq. (4).

To advance the solution of Eq. (7) in time, the Implicit-Explicit Runge-Kutta (IMEX) scheme[13] is used. This scheme consists of multiple stages and the solution of each stage for the finite-volume based LBM, omitting the index [i,j] of control volume for convenience of writing, is given by the formula;

$$f_\alpha^{(s)} = f_\alpha^n - \frac{\Delta t}{A}\sum_{k=1}^{s-1} \tilde{m}_{sk} F_\alpha{}^{(k)} - \frac{\Delta t}{\lambda}\sum_{k=1}^{s} m_{sk}(f_\alpha^{(k)} - f_\alpha^{eq,(k)}), \quad (8)$$

where *s*, $f_\alpha^{(\cdot)}$, $f_\alpha^{eq(\cdot)}$, and $F_\alpha^{(\cdot)}$ are the stage number, the stage distribution functions, the stage equilibrium distribution functions, and the stage sum of numerical fluxes, respectively. f_α^n represents the distribution functions of the time level. Then, the solution at next time level is given by;

$$f_\alpha^{n+1} = f_\alpha^n - \frac{\Delta t}{A}\sum_{j=1}^{r} \tilde{n}_j F_\alpha{}^{(j)} - \frac{\Delta t}{\lambda}\sum_{j=1}^{r} n_j(f_\alpha^{(j)} - f_\alpha^{eq,(j)}), \quad (9)$$

where *r* is the total number of stages. In addition, the *rxr* matrices of $\tilde{m}$ and *m* and the *r* vectors of $\tilde{n}$ and *n* contain the coefficients that characterize the IMEX scheme. For the present implementation, a 3-stage 2nd order form proposed by Pareschi and Russo[13] is used and to accelerate the convergence of iterations in pseudo time (subiterations), a local time stepping strategy[14] is followed. A Dual Time Stepping scheme[15] is also implemented to make the time-accurate simulation feasible allowing larger time steps that are restricted by order of accuracy desired not by the stability limit of the time advancement method.

As to model the effect of turbulence in the simulations, one-equation model of Spalart-Allmaras[16] is implemented. To solve the transport equation for the eddy-viscosity model of Spalart-Allmaras, the same cell-centered finite-volume based approach is followed that is also applied for the LBM.

2.2. Fluent Version 14.5

Fluent is a commercially available flow solver that is based on finite-volume formulation of the NS equations. The same cell-centered approach that is followed for the present implementation of the LBM is used in Fluent, too. But, contrary to the present implementation, Fluent can handle both structured and unstructured grids. The other major difference from the current LBM flow solver that Fluent can solve both incompressible and compressible flows while the LBM works only for incompressible or mildly compressible flows.

Fluent can provide second order accuracy both in time and space discretization. The second order accuracy in space is provided with the MUSCL scheme that is also used for the present implementation. A dual time stepping scheme is also available in Fluent either with an explicit Runge-Kutta or an implicit Lower Upper factorization method resulting in second order accuracy for the temporal discretization.

When using Fluent, turbulence may be taken into account using one of the many models implemented and, among them; the same Spalart-Allmaras one-equation model implemented into the LBM flow solver is also available.

3. SIMULATION DETAILS

Before beginning the simulations, a grid convergence study is performed first. For this purpose, starting from a coarse grid, three C-type structured grids were created halving the spacing between the grid points. Among them, the medium grid is shown in Fig. (2). This grid has 377 points in the chordwise direction and 171 points normal to the airfoil. The spacing between the first layer of cells wrapping the airfoil and the airfoil surface is 1.E-6 chord length. The outer boundary of the grid extends about 100 chord lengths away from the airfoil for all three grids used.

To define the adequate grid resolution, static simulations that correspond to 5 degrees angle of attack were run using the three grids generated. The variation of lift and drag coefficients with the grid resolution are given in Tbl. (1). After this study, it was concluded that the grid with 377x171 points has only %2 error in lift and %4 error in drag coefficients, thus it has enough resolution to use in further simulations.

To investigate the accuracy of the implemented method, static simulations were performed first and the computed force and moment coefficients were compared with the experimental data. Once the confidence in the implemented method was satisfied, dynamic stall simulations were performed. The dynamic stall cases considered in this study is given in Tbl. (2).

The dynamic stall simulations were started from the static solutions obtained for the mean angle of attack to reduce the number of cycles that are necessary for a converged solution. The variation of pitch angle

with time was computed using;

$$\alpha(t) = \alpha_0 + \alpha_a sin(\omega t), \quad (10)$$

where α_0 and α_a are the mean angle and the amplitude of the pitching, respectively. Ω is the frequency of the motion and *t* stands for the time. At each time step, the grid was rotated rigidly due to the above given change in the pitch angle. For all the cases, the time step was set to complete a cycle in 8000 and at the end of 2.5 cycles convergence was obtained for the monitored variations of forces and pitching moment.

4. RESULTS

As has been stated, the aim of the present study is to calculate the forces and moments of a sinusoidally pitching two dimensional airfoil by using two different numerical methods and compare results against experimental data. Initially, static stall case was performed and the obtained numerical results were compared with experimental ones and are shown in Fig. (3). The comparison between the methods and the experiment is remarkably good.

Thereafter, dynamic stall phenomenon was considered for three cases, i.e. attached flow, light stall, and deep stall. For attached flow, the force and pitching moment coefficients are depicted in Fig. (4). The solid arrow represents the upstroke and the dashed one represents the downstroke of the oscillating cycle. During the downstroke, the lift and pitching moments are higher than the upstroke values because of the formation of upwash flow. The calculated lift coefficients are in better agreement with the experiment. The computed pitching moments during upstroke is higher and the drag is lower than the experimental value. The hysteresis shapes of drag coefficients are same, but there is a shift between numerical results and the experimental data. It should be stated that the viscous components of forces and moment were not involved both in the experiment and the numerical results.

Secondly, the light stall case was considered and the comparisons of the forces and moment are shown in Fig. (5). Both methods have given acceptable results for this case. But, the results of the present method are slightly better. The difference may be explained knowing the fact that the flow is separated from the trailing edge of the airfoil along the downstroke. To investigate this, the flow field evolution computed with the two methods were compared and shown in Fig. (7). The stations along the cycle that the streamlines were computed is shown in Fig. (6). This comparison reveals that the present method retains the separation longer during the cycle thus giving better results.

Finally, the simulations of the deep stall case were performed and the comparisons of the forces and moment are shown in Fig. (8). Even though the comparison is not as good as the other two cases considered, both methods have captured the expected leading edge separation. This is shown in Fig. (9). Again, the present method retains the trailing edge separation longer thus giving slightly better results.

5. CONCLUSION AND FUTURE WORK

In this study, 2-D LBM has been implemented following the finite-volume approach in a cell-centered fashion. With the implemented flow solver, one of the most complex flow problems in rotor aerodynamics, i.e. dynamic stall, has been solved for three different flow conditions and the computed variations of force and moment coefficients with pitching angle have been compared with experimental data and the results from a NS equations based flow solver. The comparisons have revealed that the LBM, at least for this problem, can provide satisfactory results that are almost equivalent to its counterpart. As for the conclusion, the LBM has been proven to be an efficient and easy to implement alternative to the NS equations based methods.

As the future work, a 3-D version of the method is going to be implemented to study more practical flow problems related to helicopter aerodynamics such as rotor performance in hover and forward flight conditions.

REFERENCES

[1] McNamara, G. R. and Zanetti, G., “Use of the Boltzmann Equation to Simulate Lattice-Gas Automata,” Physical Review Letters, Vol. 61, 1988, pp. 2332.

[2] Thommes, G., Becker, J., Junk, M., Vaikuntam, A., and Kehrwald, D., “A Lattice Boltzmann Method for Immiscible Multiphase Flow Simulations Using the Level Set Method,” Journal of Computational Physics, Vol. 228, 2009, pp. 1139–1156.

[3] Li, X. M., Leung, R. C. K., and So, R. M. C., “One-Step Aeroacoustics Simulation Using Lattice Boltzmann Method,” AIAA Journal, Vol. 44, 2006, pp. 79–89.

[4] Chen, S., “A Large-Eddy Based Lattice Boltzmann Model for Turbulent Flow Simulation,” Applied Mathematics and Computation, Vol. 215, 2009, pp. 591–598.

[5] Fallah, M. A., Myles, V. M., Krger, T., Sritharan, K., Wixforth, A., Varnik, F., Schneider, S. W., and Schneider, M. F., “Acoustic Driven Flow and Lattice Boltzmann Simulations to Study Cell Adhesion in

Biofunctionalized -fluidic Channels with Complex Geometry," Biomicrofluidics, Vol. 4, 2010.

[6] Frisch, U., Hasslacher, B., and Pomeau, Y., "Lattice-Gas Automata for the Navier-Stokes Equation," Physical Review Letters, Vol. 56, 1986, pp. 1505–1508.

[7] McCroskey, W., Carr, L., and McAlister, K., "Dynamic stall experiments on oscillating airfoils," AIAA Journal, Vol. 14, (1), 1976, pp. 57–63.

[8] Piziali, R. A., "2-D and 3-D Oscillating Wing Aerodynamics for a Range of Angles of Attack Including Stall," NASA TM–4632, September 1994.

[9] Wang, S., Ingham, D. B., Ma, L., Pourkashanian, M., and Tao, Z., "Numerical investigations on dynamic stall of low Reynolds number flow around oscillating airfoils," Computers & Fluids, Vol. 39, (9), 2010, pp. 1529–1541.

[10] Dumlupinar, E. and Murthy, V., "Investigation of Dynamic Stall of Airfoils and Wings by CFD," AIAA Paper 2011–3511, June 2011.

[11] Fang, Y. and Menon, S., "Kinetic Eddy Simulation of Static and Dynamic Stall," AIAA Paper 2006–3847, June 2006.

[12] Leer, B. V., "Towards the Ultimate Conservative Difference Scheme. V. A Second Order Sequel to Godunov's Method," Journal of Computational Physics, Vol. 32, (1), 1979, pp. 101–136.

[13] Pareschi, L. and Russo, G., "Implicit-explicit Runge-Kutta schemes and applications to hyperbolic systems with relaxation," Journal of Scientific Computing, Vol. 25, (1-2), 2005, pp. 129–155.

[14] Imamura, T., Suzuki, K., Nakamura, T., and Yoshida, M., "Acceleration of steady-state lattice Boltzmann simulations on non-uniform mesh using local time step method," Journal of Computational Physics, Vol. 202, (2), 2005, pp. 645–663.

[15] Jameson, A., "Time dependent calculations using multigrid, with applications to unsteady flows past airfoils and wings," AIAA Paper 91–1596, June 1991.

[16] Spalart, P. R. and Allmaras, S. R., "A one equation turbulence model for aerodynamic flows," AIAA Paper 92–0439, January 1992.

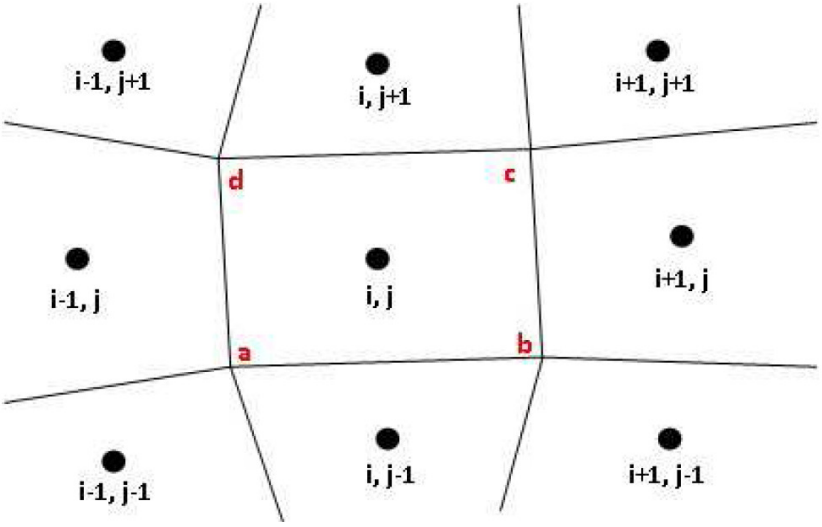

Figure 1. Quadrilateral control volumes and resulting structured grid.

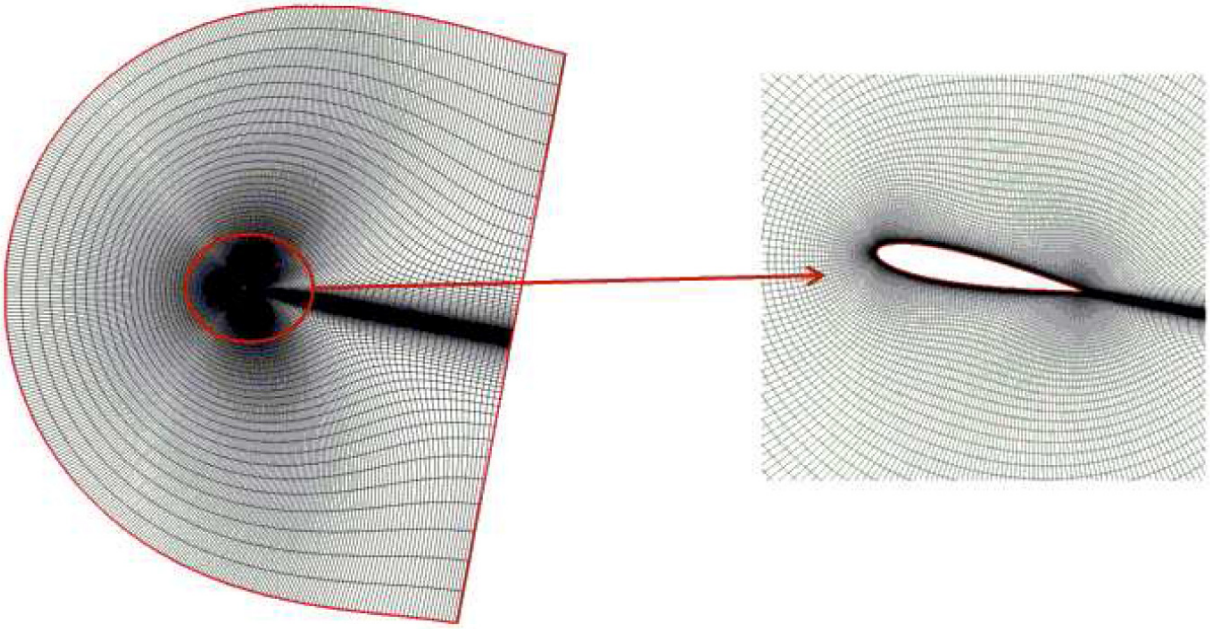

Figure 2. The C-type grid (with 377x171 points) used in the simulations.

Table 1. Results of grid convergence study performed for 5 degrees angle of attack.

Grid	Resolution	Cl	Cd	% error in Cl	% error in Cd
coarse	189x86	0.5240	0.0058	4	45
medium	377x171	0.5371	0.0041	2	4
fine	753x341	0.5445	0.0040	0	1
extrapolation	∞	0.5470	0.0040		

Table 2. Dynamic stall cases considered.

Case	Mean angle of attack (degrees)	Pitch amplitude (degrees)	Reduced frequency
attached flow	4.03	4.18	0.095
light stall	10.88	4.22	0.095
deep stall	17.04	4.14	0.096

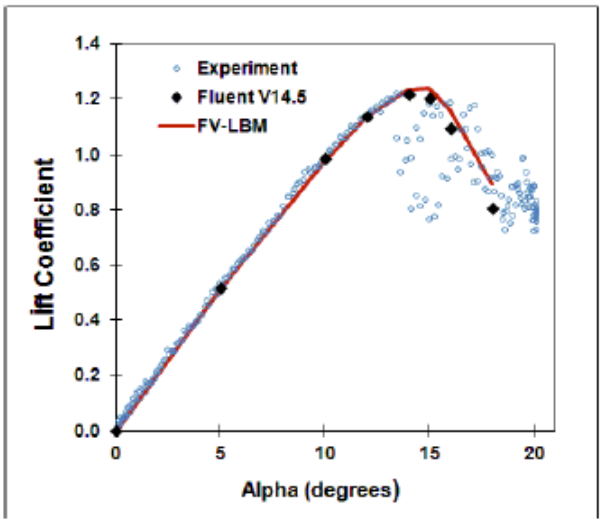

(a)

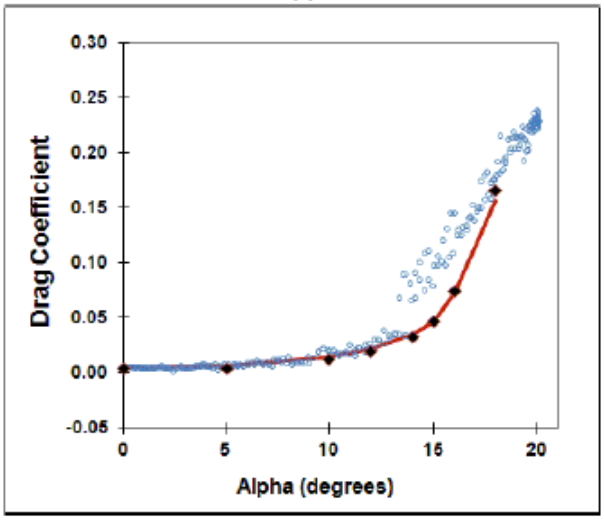

(b)

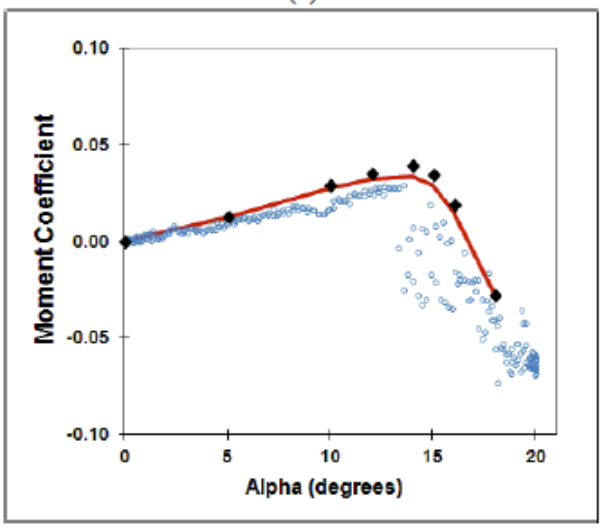

(c)

Figure 3. Comparison of computed and measured static data of (a) lift coefficient, (b) drag coefficient, and (c) moment coefficient.

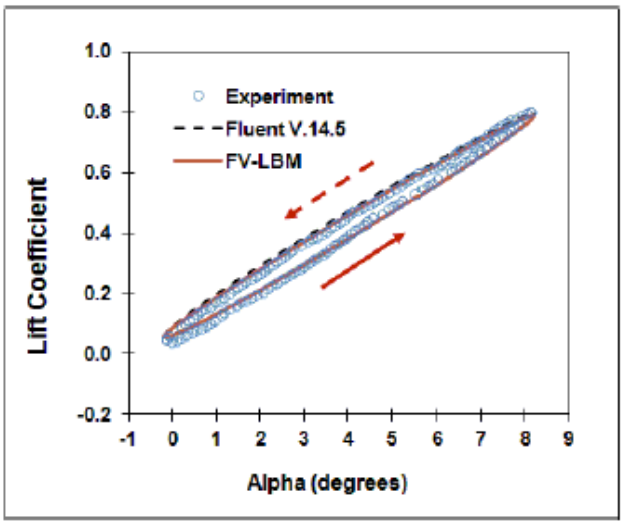

(a)

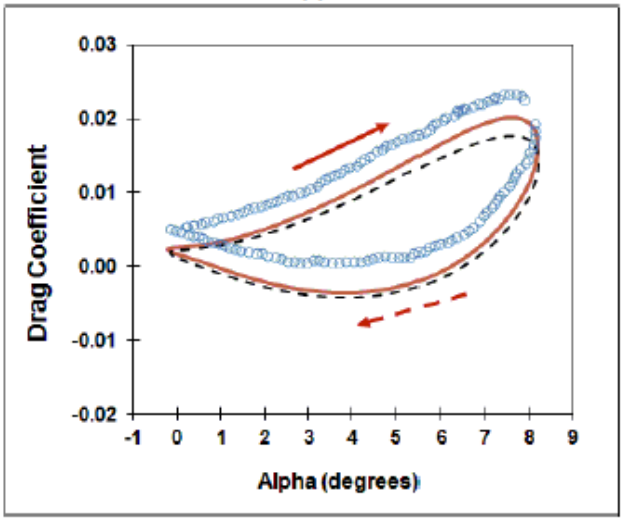

(b)

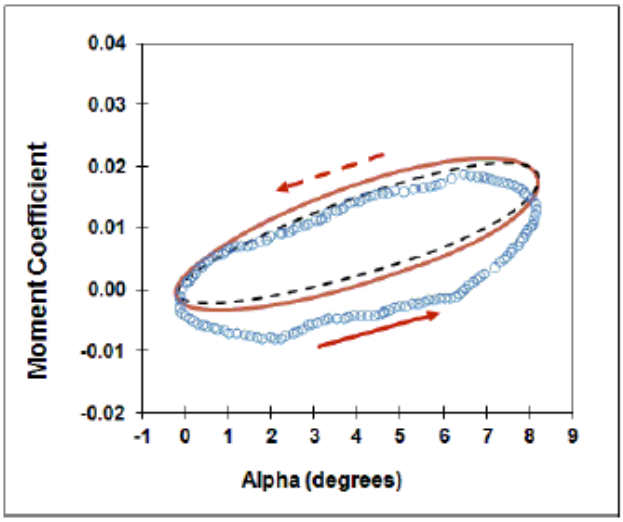

(c)

Figure 4. Comparison of pitch variation of (a) lift coefficient, (b) drag coefficient, and (c) moment coefficient for the attached flow case. (solid and dashed arrows mean upstroke and downstroke, respectively.

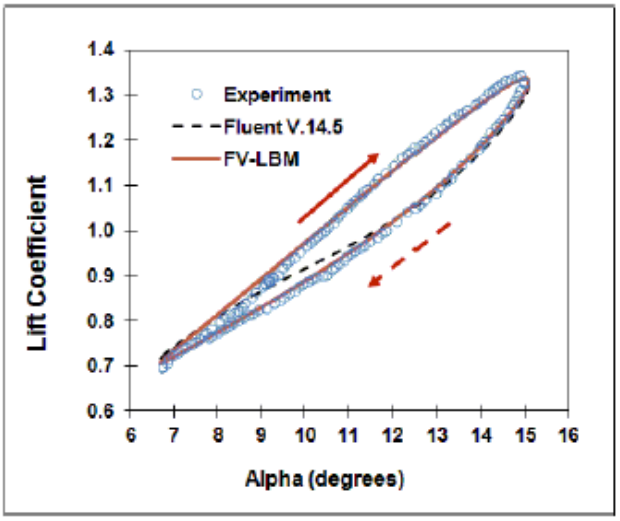

(a)

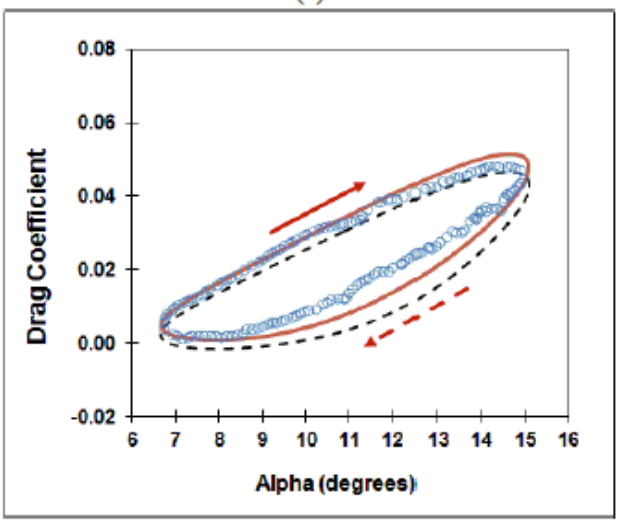

(b)

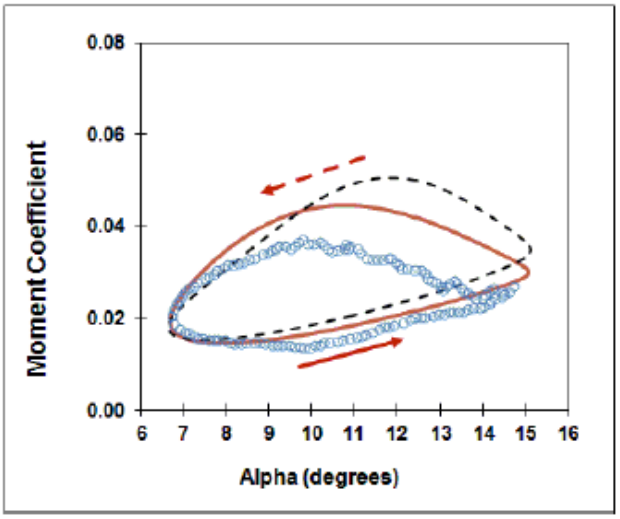

(c)

Figure 5. Comparison of pitch variation of (a) lift coefficient, (b) drag coefficient, and (c) moment coefficient for the light stall case. (solid and dashed arrows mean upstroke and downstroke, respectively.

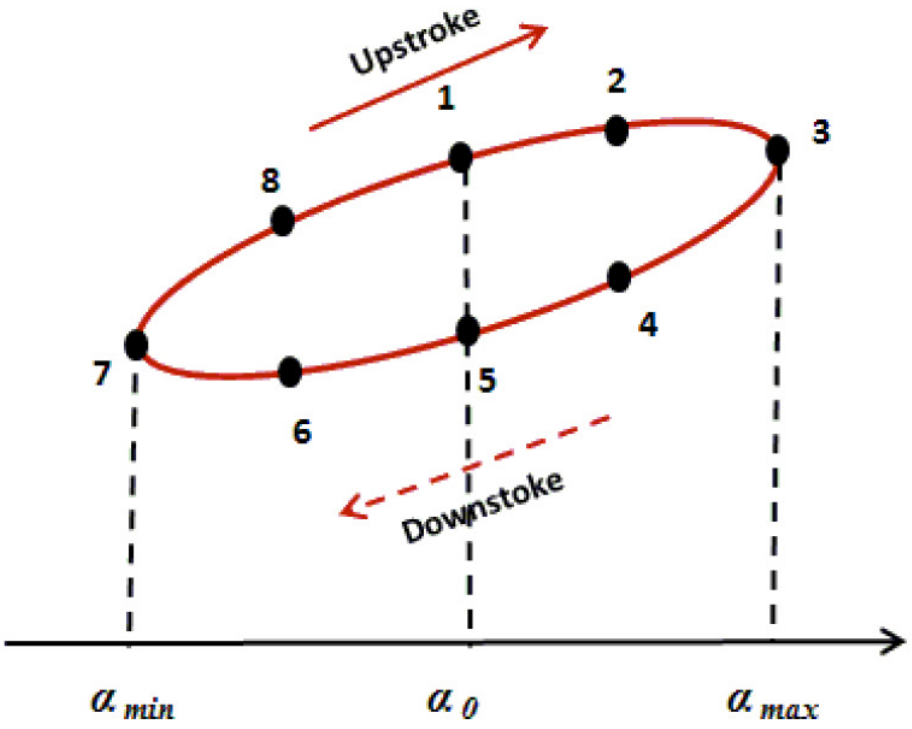

Figure 6. Points along the pitching cycle that streamlines were extracted.

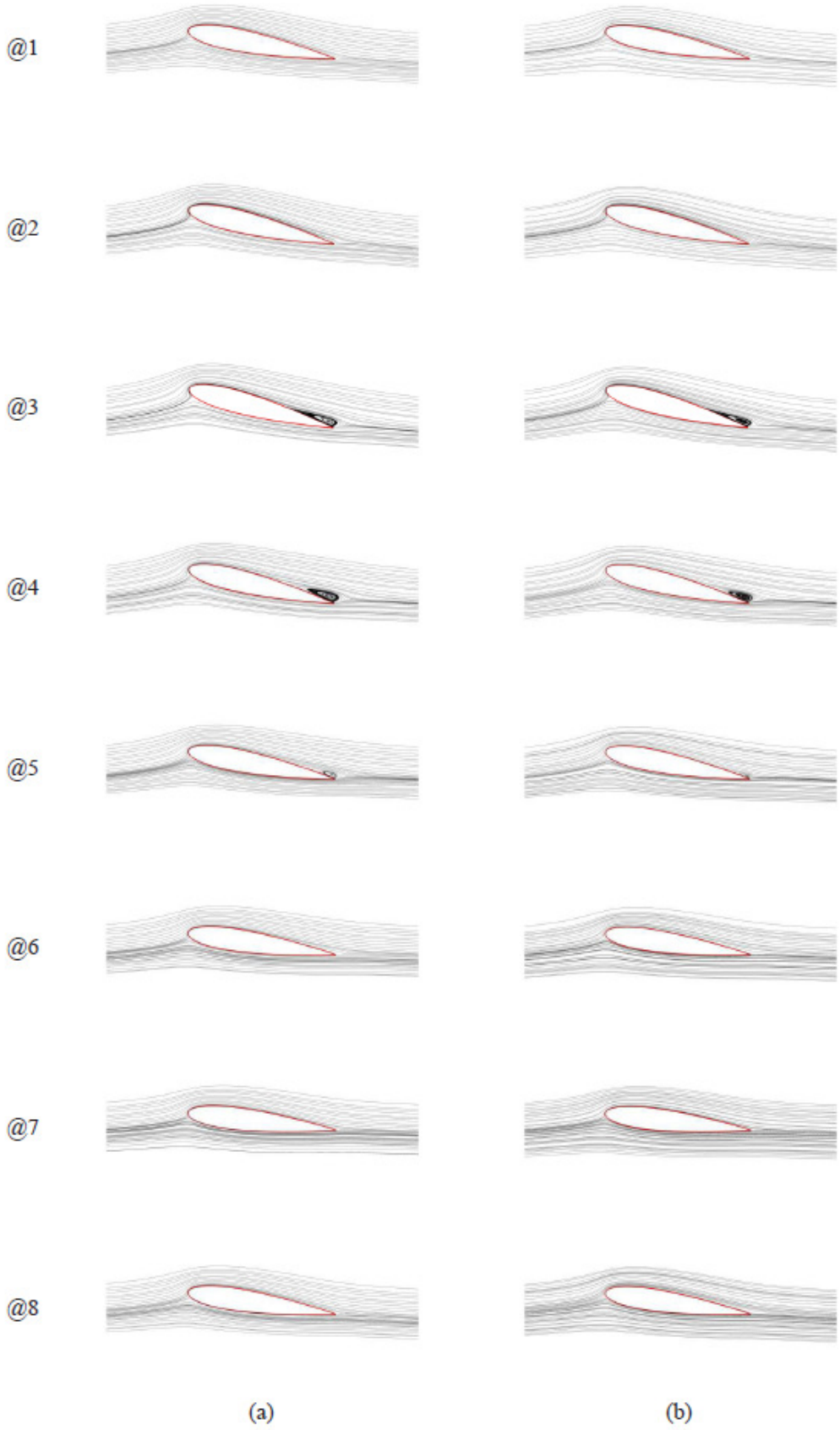

Figure 7. Comparison of the streamlines around the airfoil computed with (a) FV-LBM and (b) Fluent for the light stall case.

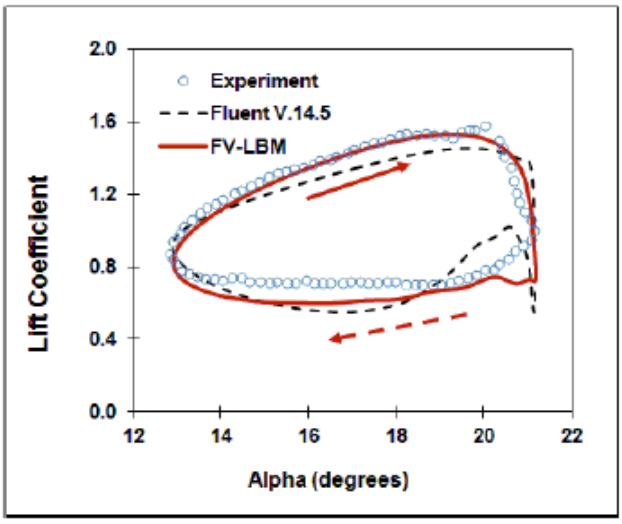

(a)

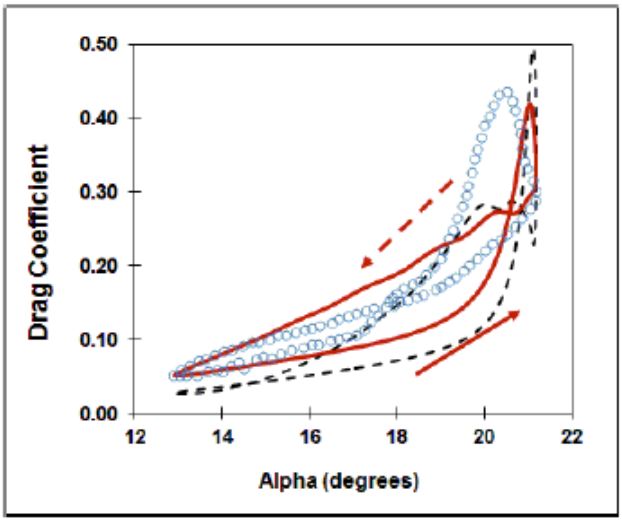

(b)

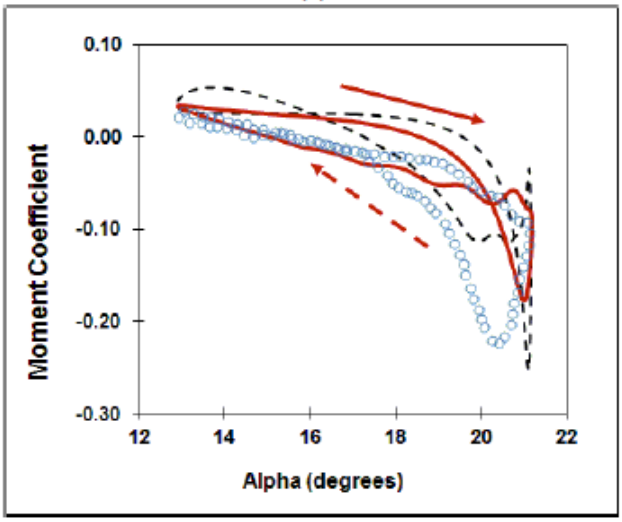

(c)

Figure 8. Comparison of pitch variation of (a) lift coefficient, (b) drag coefficient, and (c) moment coefficient for the deep stall case. (solid and dashed arrows mean upstroke and downstroke, respectively.

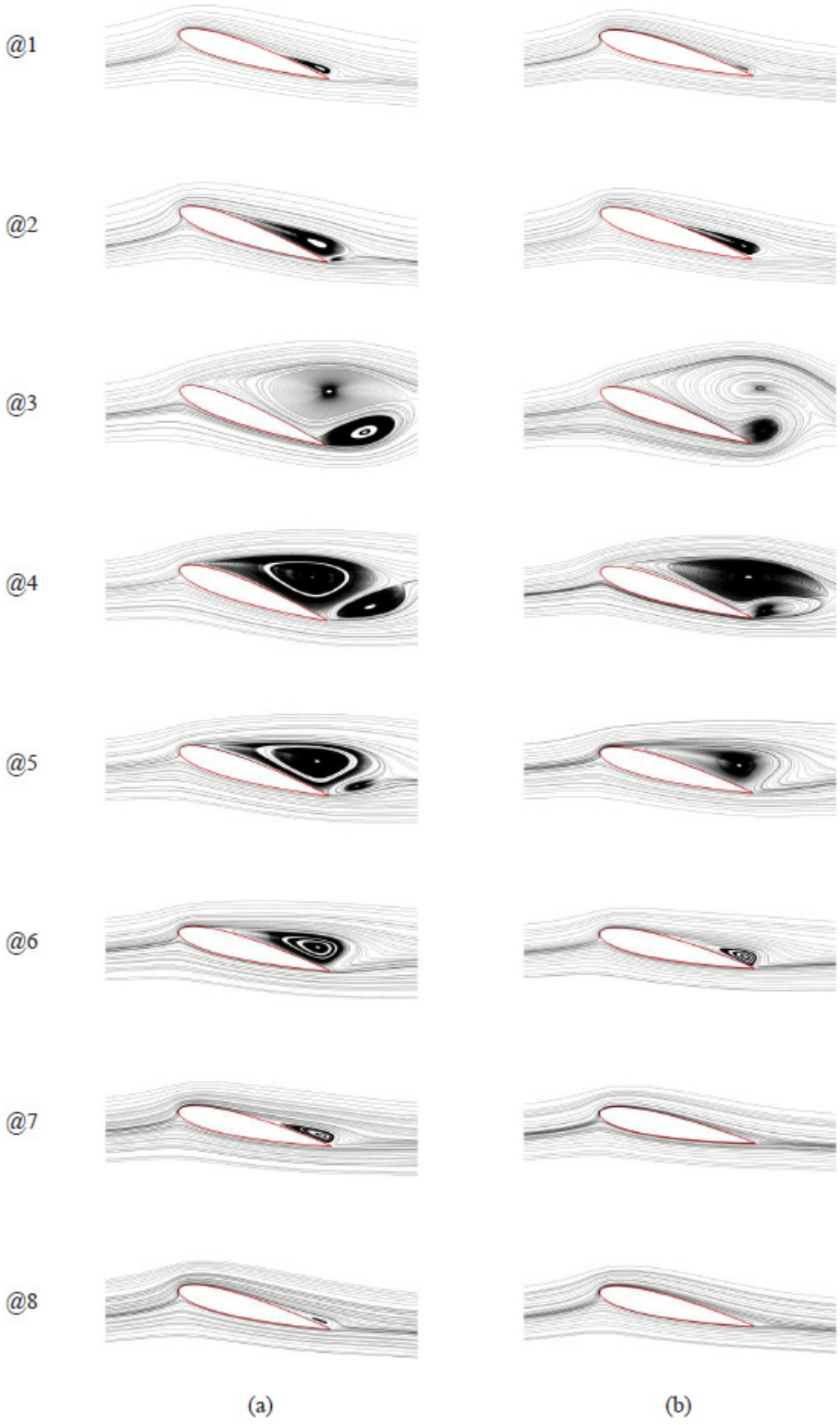

Figure 9. Comparison of the streamlines around the airfoil computed with (a) FV-LBM and (b) Fluent for the deep stall case.